Pattern Recognition Letters 85 (2017) 49–55

Contents lists available at ScienceDirect

Pattern Recognition Letters

journal homepage: www.elsevier.com/locate/patrec

A fuzzy clustering image segmentation algorithm based on Hidden Markov Random Field models and Voronoi Tessellation

Quan-hua Zhao*, Xiao-li Li, Yu Li, Xue-mei Zhao

School of Geomatics, Liaoning Technical University, Fuxin, Liaoning 123000, China

ARTICLE INFO

Article history:
Received 6 November 2015
Available online 29 November 2016

Keywords:
Voronoi Tessellation (VT)
Hidden Markov Random Model (HMRF)
Fuzzy clustering
Image segmentation

ABSTRACT

In this paper, we present new results related to the Voronoi Tessellation (VT) and Hidden Markov Random Field (HMRF) based Fuzzy C-Means (FCM) algorithm (VTHMRF-FCM) for texture image segmentation. In the VTHMRF-FCM algorithm, a VTHMRF model is established by using VT to partition an image domain into sub-regions (Voronoi polygons) and HMRF to describe the relationship of neighbor sub-regions. Based on the VTHMRF model, the objective function of VTHMRF-FCM is defined by adding a regularization term of Kullback–Leibler (KL) divergence information to FCM objective function. The proposed algorithm combines the benefits stemming from robust regional HMRF and FCM based clustering segmentation. Segmentation experiments on synthetic and real images by the proposed and other improved FCM algorithms are performed. Their results demonstrate that the proposed algorithm can obtain much better segmentation results than other FCM based methods.

1. Introduction

Segmentation is an essential process in image analysis with applications to pattern recognition, object detection, scene classification, etc., and decomposes a given image domain into homogenous regions among and in which the pixels' attributes are distinct and self-similar [14]. Up until now, a variety of well-established image segmentation techniques have been developed [1], including histogram-based, thresholding, region growing, region splitting and merging, clustering/classification, graph theoretic approach, rule-based or knowledge-driven approach, as well as some more sophisticated techniques [9,13,15,21]. Because of the diversity and complexity of natural images, designing robust and efficient segmentation algorithms is still challenging. When the problem of image segmentation is achieved by a process of classification, clustering approach is favorable. In fact, as its simplicity and efficiency, clustering approach is one of the first techniques used for the segmentation of (textured) natural images [7]. Fuzzy C-means (FCM) [4] is one of the most popular fuzzy clustering approaches that are applied successfully in image segmentation [4,17,26].

Although the original FCM algorithm provides satisfactory results for segmenting noise free images, the noises and blurs of images limit its segmentation accuracy. Its sensitivity for noises is essentially due to the absence of the information on the spatial position of pixels to be clustered. In order to circumvent the problem, many modified FCM approaches have been proposed. Ahmed et al. [2] proposed the FCM with Spatial constraints algorithm (FCM_S) by introducing a regularization term in its objective function and the regularization term is the weighted averages of the Euclidian distances from gray levels of neighbor pixels to cluster centers. One disadvantage of FCM_S is that the neighborhood labels should be computed in each iteration step. Consequently, it is very time-consuming. In order to speed up the algorithm, Chen and Zhang [9] proposed its two variants: FCM_S1 and FCM_S2, in both of which the neighborhood actions are presented by mean- and median-filtering images, respectively. Another improvement of FCM_S for reducing its execution time is the Enhance FCM (EnFCM) algorithm [24]. In EnFCM, the influence of neighbor pixels is preformed with a mean-filtering-like image, which is in advance generated from gray level of a pixel and its local neighbor average gray level. Instead of pixels of the filtering image, the clustering of EnFCM is carried out on its gray level histogram. Consequently, the computation time is considerably reduced, since in a grayscale image the number of its gray levels is much less than that of its pixels. Cai et al. [6] proposed the Fast Generalized FCM (FGFCM) algorithm. Firstly, FGFCM fuses both spatial and spectral information to define a local similarity measure. Then a new mean-filtering image is formed on the basis of the measure. In order to preserve robustness and noise insensitiveness, Krinidis and Chatzis [18] proposed the Fuzzy Local Information C-Means (FLICM) algorithm. In FLICM, a new fuzzy factor is introduced into its objective function, which incorporates the spatial and spectral information of the pixels within a local window and controls the influence of the

* Corresponding author. Fax: +86 418 3350479.
E-mail addresses: zhaoquanhua@lntu.edu.cn, zqhlby@163.com (Q.-h. Zhao).

http://dx.doi.org/10.1016/j.patrec.2016.11.019
0167-8655/

neighborhood pixels depending on theirs distances from the central pixel. Similar to FCM_S algorithm, its cluster center can also be calculated from a mean-filtering-like image which is generated with the fuzzy factor. Similarly, Xia et al. [27] proposed a Fuzzy Clustering of Spatial Patterns (FCSP) algorithm which defines dissimilarity composed of feature and spatial items in the designed neighborhood and introduced it into FCM to make the FCSP more robust to noise.

Recently, some approaches mixing statistical model into FCM algorithm have been developed. Chatzis and Varvarigou [8] dealt with Hidden MRF (HMRF) under FCM frame and developed a so-called HMRF-FCM algorithm. In the proposed algorithm, the dissimilarity function is defined with negative log-likelihood in HMRF and its objective function is formulated using Kullback–Leibler (KL) divergence information [6,22], in which the prior probabilities are obtained on the basis of the mean-field-like approximation of the HMRF. Though HMRF-FCM offers enhancement for other FCM-based segmentation algorithms to some extent, it still exhibits the disadvantage on the sensitivity of noise because only the effects from neighbor pixels are considered. In order to further enhance robustness to noise, the interactions among pixels from a large region rather than neighbors must be introduced. To this end, many region based algorithms have been proposed to segment high resolution images [10,11]. Among of them, a class of geometry tessellation-based methods is proposed [16,25]. The idea behind these methods is that the image domain is first partitioned into sub-regions by a tessellation technique, and then the extension of the HMRF model is explored to model the relationship between sub-regions instead of neighbor pixels. Li and Li [21] demonstrated that the use of a geometry tessellation based method which integrates Voronoi Tessellation (VT) [23], Bayesian inference, and Maximum A Posterior (MAP) algorithms is effective in SAR image segmentation. To introduce the region based idea into the HMRF-FCM, a VT and HMRF based FCM (VT-HMRF FCM) algorithm is proposed in this paper. The proposed algorithm explores the VT and HMRF model to define the fuzzy objective function and then utilizes the KL divergence information to regularize the defined function. It combines the benefits stemming from region based segmentation and HMRF-FCM algorithm.

This paper is organized as follows. In Section 2, the VT-HMRF model is described. In Section 3, the standard FCM, KL information based FCM are presented and VT-HMRF FCM algorithm is proposed in detail. In Section 4, the experimental evaluation of the image segmentation performance of the proposed and other FCM-based algorithms is given, and finally, the conclusion is exposed in Section 5.

2. VT-HMRF model

An observed image $\boldsymbol{z}=\{z_i\ (x_i, y_i)\colon (x_i, y_i)\in D,\ i=1, \ldots, n\}$, where i is the index of pixels, (x_i, y_i) and z_i are the site and intensity of pixel i, respectively, n is the number of pixels of $\boldsymbol{z}$, D is its domain, can be viewed as a realization of a discrete random field (called observed or feature field) defined on D, $\boldsymbol{Z}=\{Z_i\ (x_i, y_i)\colon (x_i, y_i)\in D, i=1, \ldots, n\}$, where Z_i is a random variable on (x_i, y_i). Let $\Omega_{\boldsymbol{Z}}$ be the space of all possible realizations of $\boldsymbol{Z}$.

In order to model an image $\boldsymbol{z}$ regionally, VT is used to partition its domain D into m Voronoi polygons (or sub-regions), $D=\{P_j\colon j=1, \ldots, m\}$, by m generating points $G=\{(u_j, v_j)\colon (u_j, v_j)\in D,\ j=1, \ldots, m\}$, where P_j is j'th polygon generated by generating point (u_j, v_j) and can be defined as,

$$P_j=\left\{\begin{array}{l}(x,y)\colon d\big((x,y),(u_j,v_j)\big)\le d\big((x,y),(u_{j'},v_{j'})\big),\\ (u_j,v_j),(u_{j'},v_{j'})\in G,\ j\ne j'\end{array}\right\} \tag{1}$$

where $d(\cdot,\cdot)$ is the Euclidian distance of two points in R^2.

Consider an image containing k homogenous regions (k is known *a priori*). Its domain is partitioned into m sub-regions by VT. Assign a label $L_j\in\{1, \ldots, k\}$ to P_j to indicate the homogenous region to which the polygon belongs. It implies that all pixels in P_j share the same label. Thereby, the labels of all polygons forms a label field $\boldsymbol{L}=\{L_j\colon j=1, \ldots, m\}$. Equivalently, $\boldsymbol{L}$ can also be defined on pixels, $\boldsymbol{L}=\{L_{(i)}\colon i=1, \ldots, n\}$, where $L_{(i)}$ is the label of pixel i and $L_{(i)}=L_j$ if and only if $(x_i, y_i)\in P_j$. Assume that $\boldsymbol{L}$ has a prior distribution $p(\boldsymbol{L})$, which characterizes the relationship among neighbor polygons with respect to their labels. In this paper, the stationary second-order Potts model [3] that characterizes the dependence between neighbor pixels in the vertical, horizontal and diagonal directions is extended to model the correlation of labels of neighbor polygons. Two distinct polygons P_j and $P_{j'}$ are neighbors, denoted by $P_j\sim P_{j'}$, if and only if P_j and $P_{j'}$ have a mutual boundary, where the operator $\sim$ denotes neighborhood relationship. For a given polygon P_j, let $NP_j=\{P_{j'}\colon P_{j'}\sim P_j\}$ be the set of its neighbor polygons.

Assume that the conditional distributions for labels of all polygons are independent of each other. Consequently, the joint probability density function (pdf) of $\boldsymbol{L}$ can be expressed as

$$p(\boldsymbol{L}|\beta)=\prod_{j=1}^{m}p(L_j|\beta,L_{j'},P_{j'}\in NP_j)=\prod_{j=1}^{m}\frac{\exp\left(\beta\sum\limits_{P_{j'}\in NP_j}t(L_j,L_{j'})\right)}{\sum\limits_{l=1}^{k}\exp\left(\beta\sum\limits_{P_{j'}\in NP_j}t(l,L_{j'})\right)} \tag{2}$$

where β (>0) characterizes the spatial interaction of neighbor polygons and t is the indicator function where $t(x, y)=1$ if $x=y$, otherwise, $t(x, y)=0$.

Given an observed field $\boldsymbol{Z}$, assume that the random variables Z_1, …, Z_n are independent and their pdfs depend only on the values of their label L_j, if $(x_i, y_i)\in P_j$, respectively. Assume that Z_i can be modeled by conditional Gaussian distribution with mean $\mu_{(L_i)}$and variance $\sigma^2_{(L_i)}$depending on the class to which the P_j belongs. As a result, let $\boldsymbol{\theta}=(\boldsymbol{\theta}_1, \ldots, \boldsymbol{\theta}_k)=((\mu_1, \sigma_1), \ldots, (\mu_k, \sigma_k))$, where $\boldsymbol{\theta}$ is the vector of unknown parameters.

Under those assumptions, the conditional pdf of $\boldsymbol{Z}$ given $\boldsymbol{L}$ can be written as

$$\begin{aligned}p(\boldsymbol{Z}|\boldsymbol{L},\boldsymbol{\theta})&=\prod_{j=1}^{m}\prod_{(x_i,y_i)\in P_j}p(Z_i|L_j,\boldsymbol{\theta}_{L_j})\\&=\prod_{j=1}^{m}\prod_{(x_i,y_i)\in P_j}\frac{1}{\sqrt{2\pi\sigma^2_{L_j}}}\exp\left(-\frac{(Z_i-\mu_{L_j})^2}{2\sigma^2_{L_j}}\right)\end{aligned} \tag{3}$$

Using Bayes' rule and substituting Eqs. (2) and (3), VT-HMRF model can be defined as

$$\begin{aligned}&p(\boldsymbol{L}|\boldsymbol{Z},\boldsymbol{\theta},\beta)\propto p(\boldsymbol{Z}|\boldsymbol{L},\boldsymbol{\theta})p(\boldsymbol{L}|\beta)\\&=\prod_{j=1}^{m}\prod_{(x_i,y_i)\in P_j}\frac{1}{\sqrt{2\pi\sigma^2_{L_j}}}\exp\left(-\frac{(Z_i-\mu_{L_j})^2}{2\sigma^2_{L_j}}\right)\times\prod_{j=1}^{m}\frac{\exp\left(\beta\sum\limits_{P_{j'}\in NP_j}t(L_j,L_{j'})\right)}{\sum\limits_{l=1}^{k}\exp\left(\beta\sum\limits_{P_{j'}\in NP_j}t(l,L_{j'})\right)}\end{aligned} \tag{4}$$

Eq. (4) provides an approximation of the posterior probability $p(\boldsymbol{L}|\boldsymbol{Z})$ and guarantees its Markovianity, though more complicated assumptions can be employed [5].

3. VT-HMRF FCM algorithm

3.1. Standard FCM model

The standard FCM based image segmentation algorithm [4] partitions the image $\boldsymbol{z}$ into k clusters by iteratively minimizing the following objective function

$$J_{FCM} = \sum_{l=1}^{k}\sum_{i=1}^{n} r_{(li)}^{\xi} d_{(li)}^2 \tag{5}$$

where $d_{(li)} = ||z_i - v_l||_2$ is the Euclidean distance between pixel intensity z_i and the prototype (or cluster center) of the lth cluster v_l, the fuzzifier of the clustering ξ is the weighting exponent on fuzzy memberships and controls the degree of fuzziness, $r_{(li)}$ is the fuzzy membership of the ith pixel belonging to the lth cluster, subject to $r_{(li)} \in [0, 1]$, $\forall i = 1, \ldots, n$, and $l = 1, \ldots, k$, $\sum_{l=1}^{k} r_{(li)} = 1$, $\forall i = 1, \ldots, n$; $0 < \sum_{i=1}^{n} r_{(li)} < n$, $\forall l = 1, \ldots, k$. Minimizing Eq. (5) under the above constraints, the fuzzy membership functions $r_{(li)}$ and cluster center v_l can be calculated [4].

3.2. KL information based FCM

Since the fuzzifier ξ in J_{FCM} is introduced as the exponent on fuzzy membership, the fuzzy objective function J_{FCM} seems to be rather unnatural [20]. There are several algorithms proposed to improve the FCM clustering. Miyamoto and Mukaidono [22] suggested that fuzzification can be obtained by means of a regularization technique where an entropy term is added into the fuzzy objective function as follows,

$$J_{EN} = \sum_{l=1}^{k}\sum_{i=1}^{n} r_{(li)} d_{(li)} + \lambda \sum_{l=1}^{k}\sum_{i=1}^{n} r_{(li)} \log r_{(li)} \tag{6}$$

where the entropy term acts as the fuzzifier and the parameter λ decides the fuzzy degree of clustering model. Ichihashi et al. [19] proposed another FCM variant by introducing a regularization term with KL information. Under this consideration, the fuzzy objective function is defined as

$$J_{KL} = \sum_{l=1}^{k}\sum_{i=1}^{n} r_{(li)} d_{(li)} + \lambda \sum_{l=1}^{k}\sum_{i=1}^{n} r_{(li)} \log \frac{r_{(li)}}{\pi_{(li)}} \tag{7}$$

where $\pi_{(li)}$ is the prior probability (weight) of ith pixel belonging to lth cluster.

3.3. VT-HMRF based FCM algorithm

In order to design regionalized fuzzy clustering algorithm, a new FCM objective function is defined by combining VT-HMRF model into the regularized KL information fuzzy objective function in Eq. (7). Analogy to the definition of the label field $\boldsymbol{L}$ on polygons and pixels, the membership function is also defined on them, i.e., for the P_j to affirm the feature class l with the membership r_{lj}, it means that all pixels in P_j share the same membership r_{lj}. Furthermore, their memberships to the class l can be denoted as

$$r_{(li)} = r_{lj} \Leftrightarrow (x_i, y_i) \in P_j \tag{8}$$

Instead of using Euclidean distance, the dissimilarity function $d_{(li)}$ is defined as the negative log-likelihood of pixel Z_i with $L_{(i)} = l$, that is,

$$d_{(li)} = -\log p(Z_i | \mu_{L_{(i)}=l}, \sigma_{L_{(i)}=l}) \tag{9}$$

The prior probabilities of pixels i in P_j for the lth class $\pi_{(li)}$ are the same, that is, $\pi_{(li)} = \pi_{lj} \Leftrightarrow (x_i, y_i) \in P_j$, which can be obtained by the distribution of the label L_j conditional on the labels of its neighbor polygons

$$\pi_{lj} \triangleq p(L_j = l | L_{j'}, j' \in NP_j) = \frac{\exp\left(\beta \sum_{P_{j'} \in NP_j} t(L_j = l, L_{j'})\right)}{\sum_{l'=1}^{k} \exp\left(\beta \sum_{P_{j'} \in NP_j} t(L_j = l', L_{j'})\right)} \tag{10}$$

Combine Eqs. (8)–(10), the objective function in Eq. (7) can be rewritten as

$$J_{VH} = \sum_{l=1}^{k}\sum_{j=1}^{m}\left[r_{lj} D_{lj}\right] + \lambda \sum_{l=1}^{k}\sum_{j=1}^{m}\left[N_j r_{lj} \log \frac{r_{lj}}{\pi_{lj}}\right] \tag{11}$$

where $N_j = \#\{(x_i, y_i) \in P_j\}$ is the number of pixels in P_j, and

$$D_{lj} = \sum_{(x_i, y_i) \in P_j} d_{(li)} = \sum_{(x_i, y_i) \in P_j} p(Z_i | L_j = l, \mu_l, \sigma_l^2) \tag{12}$$

3.4. Model parameters estimation

The estimation of VT-HMRF FCM parameters, $\psi = \{\boldsymbol{R}, \boldsymbol{\theta}, \boldsymbol{G}\}$, where $\boldsymbol{R} = [r_{lj}]_{k \times m}$ and $\boldsymbol{G} = \{(u_j, v_j): j = 1, \ldots, m\}$, can be carried out by iteratively minimizing the fuzzy objective function in Eq. (11) over $\boldsymbol{R}$, $\boldsymbol{\theta}$ and $\boldsymbol{G}$, respectively. Let $\psi^{(t)}$ stands for the parameters of tth iteration. In $t+1$th iteration, it is necessary to obtain an estimation of the prior probabilities ${\pi_{lj}}^{(t)}$ using Eq. (10), in which $\boldsymbol{L}^{(t)}$ can be obtained by the defuzzification of the fuzzy memberships ${r_{lj}}^{(t)}$

$${L_j}^{(t)} = \arg\max_{l=1}^{k} \left\{{r_{lj}}^{(t)}\right\} \tag{13}$$

After acquiring π_{lj}, the model parameters $\psi = \{\boldsymbol{R}, \boldsymbol{\theta}, \boldsymbol{G}\}$ can be derived as follows.

- Calculating the fuzzy membership

The fuzzy membership can be attained by minimizing the objection function in Eq. (11) over r_{lj} under the constraint $\sum_{l=1}^{k} r_{lj} = 1$ $\forall\, j = 1, \ldots, m$. Introduce a Lagrange multiplier η_l for each polygon to enforce the constraint, have

$$\frac{\partial}{\partial r_{lj}}\left[J_{VH} - \sum_{j=1}^{m} \eta_l \left(\sum_{l'=1}^{k} r_{l'j} - 1\right)\right] = 0 \tag{14}$$

which eventually yields

$$\begin{aligned} {r_{lj}}^{(t+1)} &= \frac{{\pi_{lj}}^{(t)} \exp\left(-\frac{1}{\lambda N_j} {D_{lj}}^{(t)}\right)}{\sum_{l'=1}^{k} {\pi_{l'j}}^{(t)} \exp\left(-\frac{1}{\lambda N_j} {D_{l'j}}^{(t)}\right)} \\ &= \frac{{\pi_{lj}}^{(t)} \exp\left(-\frac{1}{\lambda N_j} \sum_{(x_i, y_i) \in P_j} {d_{(li)}}^{(t)}\right)}{\sum_{l'=1}^{k} {\pi_{l'j}}^{(t)} \exp\left(-\frac{1}{\lambda N_j} \sum_{(x_i, y_i) \in P_j} {d_{(l'i)}}^{(t)}\right)} \end{aligned} \tag{15}$$

where

$$\begin{aligned} {d_{(li)}}^{(t)} &= -\log p\left(Z_i | {L_j}^{(t)} = l, {\mu_l}^{(t)}, {\sigma_l}^{(t)}\right) \\ &= \frac{1}{2}\log(2\pi) + \log {\sigma_l}^{(t)} + \frac{\left(Z_i - {\mu_l}^{(t)}\right)^2}{2\left({\sigma_l}^{(t)}\right)^2} \end{aligned} \tag{16}$$

- Calculating the model parameters

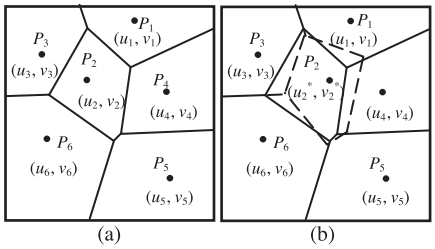

Fig. 1. (a) Voronoi tessellation with six generating points, (b) Voronoi tessellation after moving generating point (u_2, v_2) to (u_2^*, v_2^*).

To obtain the estimations of the model parameters μ_l and σ_l, the objective function is rewritten as Eq. (17) by substituting Eq. (12) into Eq. (11),

$$J_{VH} = \sum_{l=1}^{k}\sum_{j=1}^{m} r_{lj} \sum_{(x_i,y_i)\in P_j} \left[\frac{1}{2}\log(2\pi) + \log\sigma_l + \frac{(Z_i-\mu_l)^2}{2(\sigma_l)^2} \right] + \lambda \sum_{l=1}^{k}\sum_{j=1}^{m} \left[N_j r_{lj} \log \frac{r_{lj}}{\pi_{lj}} \right] \tag{17}$$

Then conduct the minimization of Eq. (17) over $\mu_l{}^{(t)}$ and $(\sigma_l{}^{(t)})^2$, have

$$\mu_l{}^{(t+1)} = \frac{\sum_{j=1}^{m} \left(r_{lj}{}^{(t+1)} \sum_{(x_i,y_i)\in P_j} Z_i \right)}{\sum_{j=1}^{m} \left(N_j r_{lj}{}^{(t+1)} \right)} \tag{18}$$

$$\left(\sigma_l{}^{(t+1)}\right)^2 = \frac{\sum_{j=1}^{m} r_{lj}{}^{(t+1)} \sum_{(x_i,y_i)\in P_j} \left(Z_i - \mu_l{}^{(t+1)}\right)^2}{\sum_{j=1}^{m} \left(N_j r_{lj}{}^{(t+1)} \right)} \tag{19}$$

- Updating $\boldsymbol{G}$

Find a new VT to minimize the objective function defined in Eq. (11). Randomly select a generating points from $\boldsymbol{G}^{(t)} = \{(u_1{}^{(t)}, v_1{}^{(t)}), \ldots, (u_m{}^{(t)}, v_m{}^{(t)})\}$, say $(u_j{}^{(t)}, v_j{}^{(t)})$. Move $(u_j{}^{(t)}, v_j{}^{(t)})$ to a candidate position $(u_j^*, v_j^*) \in P_j$. As a result, the new collection of generating points is $\boldsymbol{G}_m{}^* = \{(u_1{}^{(t)}, v_1{}^{(t)}), \ldots, (u_j^*, v_j^*), \ldots, (u_m{}^{(t)}, v_m{}^{(t)})\}$. Accordingly, P_j is changed to P_j^*. It is noteworthy that moving a generating point (u_j, v_j) will change both of P_j and its neighbor polygons. Fig. 1 shows an example of the changes of Voronoi polygons when (u_2, v_2) move to (u_2^*, v_2^*), where the solid lines denote the boundaries of Voronoi polygons and the dash lines in Fig. 1(b) are variant boundaries. Accordingly, when VT changes, the dissimilarity d_{lj} and fuzzy membership r_{lj} of the varied polygons, and corresponding the model parameters should be recalculated with Eqs. (15), (16), (18) and (19), respectively. After that, the objective function of VT-HMRF FCM can be calculated according to Eq. (11), if $J_V(\boldsymbol{G}_m{}^*) < J_V(\boldsymbol{G}^{(t)})$, the moving operation will be accepted and $\boldsymbol{d}^{(t)} = (d_{(li)}{}^{(t)}: l = 1, \ldots, k, i = 1, \ldots, n)$, $\boldsymbol{r}^{(t)} = (r_{lj}{}^{(t)}: l = 1, \ldots, k, j = 1, \ldots, m)$ and $\boldsymbol{\theta}^{(t)}$ are updated.

3.5. Summary of VT-HMRF FCM algorithm

The proposed algorithm can be summed up as follows.

- Generating m initial generating points $\boldsymbol{G}^{(0)} = \{(u_j{}^{(0)}, v_j{}^{(0)}): j = 1, \ldots, m\}$ and the initial $\boldsymbol{P}^{(0)} = \{P_j{}^{(0)}: j = 1, \ldots, m\}$ from $\boldsymbol{G}^{(0)}$.
- Initializing fuzzy membership $r_{lj}{}^{(0)}$ randomly.
- Defuzzifying the fuzzy membership $r_{lj}{}^{(t)}$ to determine the label field $\boldsymbol{L}^{(t)}$ and calculate prior probability $\pi_{lj}{}^{(t)}$ using Eq. (10).
- Calculating the fuzzy membership $r_{lj}{}^{(t)}$ by Eq. (15).
- Estimating the parameters $\boldsymbol{\mu}^{(t)} = \{\mu_1{}^{(t)}, \ldots, \mu_k{}^{(t)}\}$ and $\boldsymbol{\sigma}^{(t)} = \{\sigma_1{}^{(t)}, \ldots, \sigma_k{}^{(t)}\}$ by Eqs. (18) and (19), respectively.
- Updating $\boldsymbol{G}$ to obtain the optimal tessellation.
- If $|J_{VH}{}^{(t)} - J_{VH}{}^{(t-1)}| < T_c$, T_c is a threshold, exit iteration, otherwise, set $t = t+1$ and return to the third step.

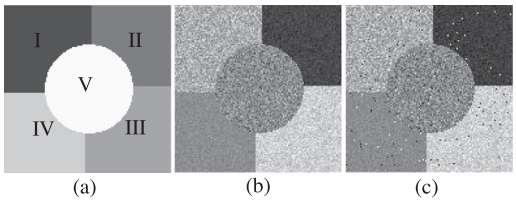

Fig. 2. (a) Template, (b) Simulated image, (c) Simulated image with Salt & pepper noise.

Table 1
Means and standard deviations of Gaussian distributions.

parameters	Region				
	I	II	III	IV	V
mean	160	40	200	120	120
std.	30	10	20	10	30

4. Experimental results and discussions

The proposed method is applied to simulated and real images. In addition, some comparisons to the performances of pixel and neighbor based FCM segmentation methods have been done. In the experiment, the parameter β is set as 0.5, λ is set as 0.04, T_c is set as 0.001 and the maximum iteration is set as 5000 for all tested images. In practice, the number of polygons m could be set as a variable, but from our experiments, within a certain range (from 48 to 128 for 128×128 images), the number has not significantly effect on segmentation results and variable m is very time consuming. In this experiment, m is taken as 96. Under the environment of IntelCore22.53 Ghz/1 G memory, the segmentation takes about 15 min for 128×128 images, and the complexity of the proposed algorithm is $O(N^2)$.

4.1. Simulated image segmentation

A quantitative evaluation of segmentation algorithms can only be effectuated on simulated images, as one needs to know the exact regions in advance. To this end, the simulated image is generated as in Fig. 2(b). It consists of five statistically homogeneous regions as in the template image Fig. 2(a), in each of which the pixel intensities follow an Gaussian distribution with mean and standard deviation listed in Table 1. In Fig. 2(b), region V and VI have same mean value, while region II and IV have same standard deviation. Fig. 2(c) shows image with the salt & pepper noises added on Fig. 2(b) with density of 0.01.

Fig. 3 shows the histograms of each homogeneous regions in Fig. 2(b), it can be seen that some of histograms have moderate overlap with each other.

Fig. 4(a1)–(a3) and (b1)–(b3) illustrates VT and segmentation results of Fig. 2(b) at the 1000 iteration, 3000 iteration, and the final state (at 5000 iterations), respectively, Fig. 4(a4) and (b4) illustrates VT and segmentation results of Fig. 2(c) at final state where each polygon is displayed with a color randomly selected. It can be seen from Fig. 4(b1)–(b4), at 1000th iteration each homogenous

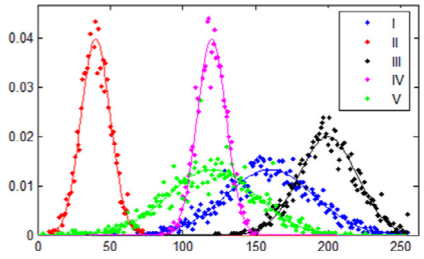

Fig. 3. Histogram of different homogeneous regions.

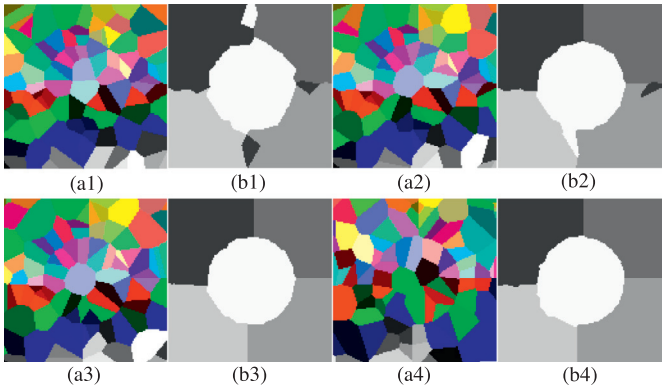

Fig. 4. (a1)–(a3) Tessellation results of Fig. 2(b) with 1000, 3000, final iterations, respectively; (b1)–(b3) Segmentation results of Fig. 2(b) with 1000, 3000, final iterations, respectively; (a4)–(b4) Tessellation and segmentation results of Fig. 2(c), respectively.

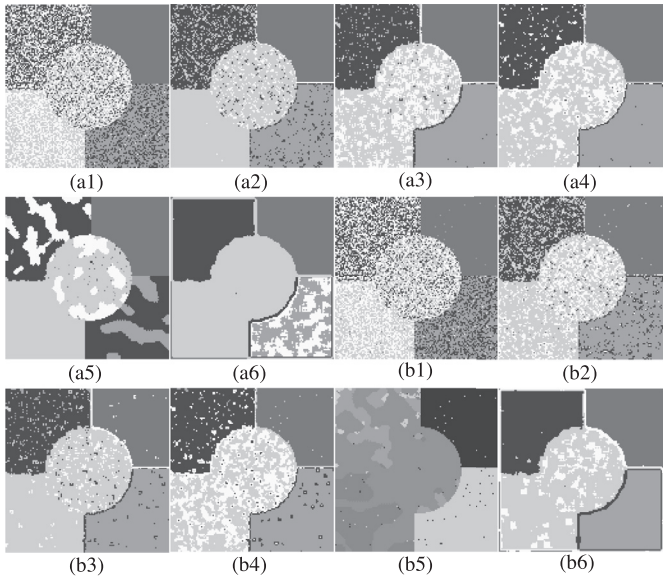

Fig. 5. (a1)–(a6) Segmentation results of Fig. 2(b) by FCM, EnFCM, FGFCM, FLICM, HMRF-FCM, K-means; (b1)–(b6) Segmentation results of Fig. 2(c) by FCM, EnFCM, FGFCM, FLICM, HMRF-FCM, K-means.

region can be segmented roughly, after 3000 iterations the result becomes more accurate, at 5000 iterations the results are excellent in the experiment, and the result of Fig. 2(c) is also excellent. Because the proposed algorithm introduces the regional effect, so it enhances robustness and noise insensitiveness, as a result, it segments different regions well and there are no obvious misclassified pixels.

Fig. 5(a1)–(a6) and (b1)–(b6) show respectively the segmentation results of image of Fig. 2(b) and (c) using FCM [4], EnFCM [24], FGFCM [6], FLICM [18] and HMRF-FCM [8] and mean filter followed by K-means clustering algorithm. All above algorithms can not distinguish region V and IV because the two regions have the same mean value. Besides, the results from the FCM in Fig. 5(a1) and (b1) are unacceptable since only pixel itself is taken into account in FCM algorithm. By contrast, Fig. 5(a2)–(a5) and (b2)–(b5) are better than Fig. 5(a1) and (b1) because the spatial context can pay a critical role in image segmentation. Fig. 5(a6) and (b6) can segment region I, II and III well because before segmentation, median filter is adopted on original image.

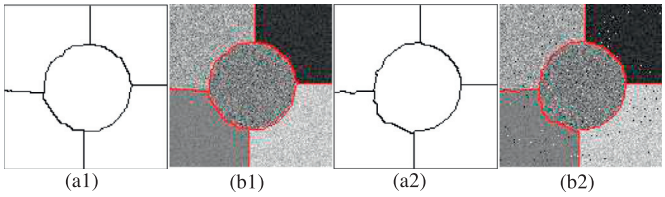

Fig. 6. (a1) and (a2) outlines of segmented regions of Fig. 2(b) and (c); (b1) and (b2) outlines overlaid on original image.

Table 2
Expectation and variance estimated of Gaussian distribution parameters.

Parameters	Region				
	I	II	III	IV	V
Estimated means & their errors (non-noise / noise)	159.39/ 159.28 (0.4%/ 0.4%)	39.88/ 39.87 (0.3%/ 0.3%)	199.76/ 199.66 (0.1%/ 0.2%)	119.76/ 119.77 (0.2%/ 0.2%)	120.14/ 119.95 (0.1%/ 0.04%)
Estimated std. & their errors(non-noise / noise)	29.79/ 29.82 (0.7%/ 0.6%)	10.27/ 10.28 (2.7%/ 2.8%)	20.34/ 20.61 (1.7%/ 3.0%)	10.08/ 10.05 (0.8%/ 0.5%)	30.79/ 30.15 (2.6%/ 0.5%)

To visually illustrate the accuracy of the segmented results of the proposed algorithm, the outlines of the segmented homogenous regions are delineated and overlaid on the simulated images Fig. 2(b) and (c), as shown in Fig. 6(a1), (a2) and (b1), (b2), respectively. Fig. 6 illustrates that the delineated outlines match well the boundaries of the homogeneous regions.

Table 2 lists the estimated Gaussian distribution parameters and their percentage errors. The maximum percentage error is only 3% for segmentation results of Fig. 2(b) and (c). The results listed in Table 2 indicate that the proposed algorithm can accurately estimate the model parameters for both non-noise image and the noise image.

In order to perform accuracy estimations quantitatively, the confusion matrix is calculated in terms of the segmentation results shown in Fig. 5 and the segmentation results by the proposed algorithm shown in Fig.(b3) and (b4). A direct comparison segmented regions with their corresponding real homogenous regions is the most commonly used schemes. Accordingly, the measurements such as producer's accuracy, consumer's accuracy, overall accuracy and Kappa coefficient, can be calculated and listed in Table 3. From Table 3, the accuracy measurements of the proposed algorithm are higher than that for all others, and the overall accuracy and the kappa coefficient are up to 99% and 0.99, respectively. General interpretation rules to assess thematic accuracy indicate that a Kappa coefficient between 0.81 and 1.0 is almost perfect [12].

4.2. Real image segmentation

Fig. 7 shows real images for testing purpose. Fig. 7(a) is an optical image with different textures and Fig. 7(b) is a SAR intensity image with RADARSAT II HH polarization, in which dark, bright and gray areas correspond to the sea, urban and forest.

Table 3
Comparison of accuracies and kappa values.

Algorithm	Measurement	Region				
		I	II	III	IV	V
FCM (non-noise/noise)	U (%)	49.9/47.5	92.4/90.3	80.5/79.6	46.1/46.2	33.7/33.6
	P (%)	44.3/43.2	100/99.5	68.3/63.4	52.2/51.5	25.9/36.9
	O (%) = 58.9/57.5; kappa = 0.49/0. 47					
EnFCM (non-noise/noise)	U (%)	83.3/80.3	99.9/98.7	93.5/92.6	45.4/42.7	88.8/63.9
	P (%)	72.9/63.6	98.1/65.8	90.1/86.2	99.9/76.5	13.3/37.3
	O (%) = 72.8/71.2; kappa = 0.66/0. 64					
FGFCM (non-noise/noise)	U (%)	93.8/90.6	99.9/99.9	96.2/95.1	48.8/47.5	60.4/70.9
	P (%)	90.2/88.2	97.8/96.1	96.9/95.2	70.0/97.2	40.9/11.9
	O (%) = 78.3/75.9; kappa = 0.730. 70					
FLICM (non-noise/noise)	U (%)	95.5/90.5	99.9/99.9	98.9/98.5	52.8/49.3	62.4/53.8
	P (%)	91.4/90.0	98.3/97.8	96.7/92.9	79.4/60.6	40.4/47.3
	O (%) = 80.2/77.1; kappa = 0.75/0. 71					
HMRF FCM (non-noise/noise)	U (%)	51.0/75.9	98.6/98.4	97.4/93.9	54.7/95.8	52.7/49.1
	P (%)	70.4/29.7	100/99.5	30.0/99.1	100/61.8	29.2/89.1
	O (%) = 64.2/75.5; kappa = 0.55/0. 69					
K-means (non-noise/noise)	U (%)	89.8/89.2	95.7/96.8	100/100	41.7/44.9	0/54.4
	P (%)	90.3/89.5	97.9/97.3	40.5/87.5	95.1/81.6	0/22.5
	O (%) = 64.0/74.2; kappa = 0.55/0. 68					
VT-HMRF FCM (non-noise/noise)	U (%)	99.4/99.0	100/100	99.9/99.9	99.6/100	98.5/96.8
	P (%)	99.6/99.6	99.6/99.7	99.5/99.8	99.1/96.5	99.4/99.4
	O (%) = 99.5/99.0; kappa = 0.99/0. 99					

U: user precision, P: product precision, O: overall precision.

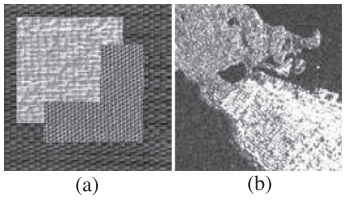

Fig. 7. (a) Texture image, (b) SAR image.

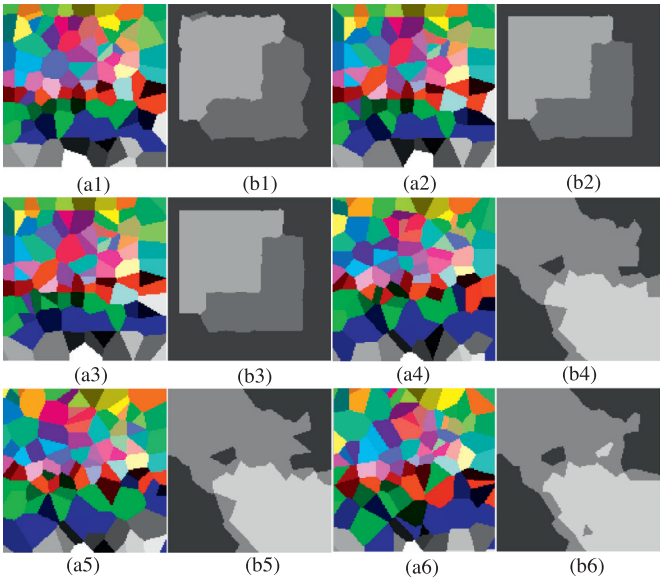

Fig. 8. (a1)–(a3) Tessellation results of Fig. 7(a) with 1000, 3000, final iterations, respectively, (b1)–(b3) Segmentation results of Fig. 7(a) with 1000, 3000, final iterations, respectively; (a4)–(a6) Tessellation results of Fig. 7(b) with 1000, 3000, final iterations, respectively; (b4)–(b6) Segmentation results of Fig. 7(b) with 1000, 3000, final iterations, respectively,.

Fig. 8 shows the tessellation and segmentation results of Fig. 7. Fig. 8(a1)–(a3) are the tessellation results at 1000, 3000 iterations and final state(at 5000 iteration) of Fig. 7(a), respectively, and Fig. 8(b1)–(b3) are the corresponding segmented results of

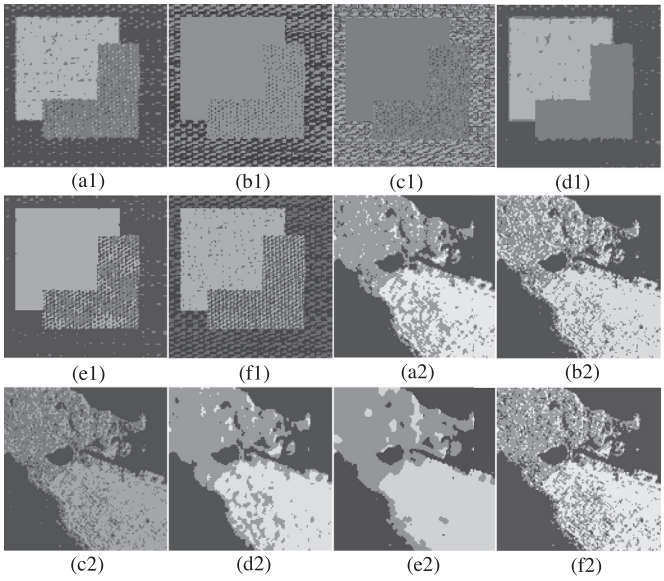

Fig. 9. (a1)–(a6) Segmentation results of Fig. 7(a) by FCM, EnFCM, FGFCM, FLICM, HMRF-FCM, K-means, (b1)–(b6) Segmentation results of Fig. 7(b) by FCM, EnFCM, FGFCM, FLICM, HMRF-FCM, K-means.

Fig. 8(a1)–(a3), Fig. 8(a4) and (b4) are the tessellation and segmentation results at final state of Fig. 7(b). As shown in Fig. 8, the segmentation results are excellent and become stable soon.

Fig. 9 shows the segmentation results of Fig. 7(a) and (b) by the classical FCM based and k-mean clustering algorithm. Fig. 9(a1)–(f1) and (a2)–(f2) are the segmentation results by FCM, EnFCM, FGFCM, FLICM, HMRF-FCM and k-means, respectively. Combined Fig. 8, It can be seen that for these images the proposed algorithm is robust and can segment different textures very well and can provides significantly better performance than other FCM-based and k-means algorithms.

Fig. 10 gives the results from other real images obtained by the proposed algorithm. It can be seen that for these images the pro-

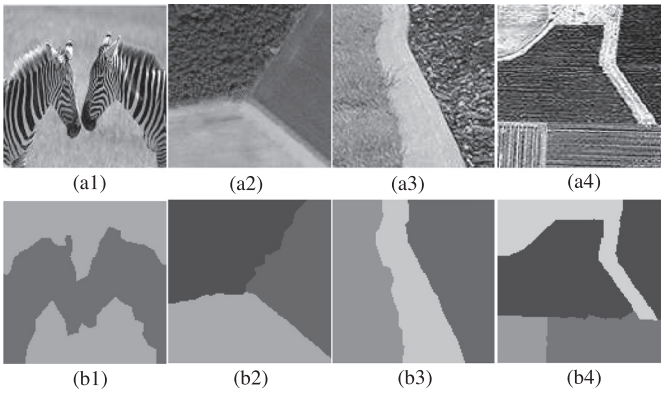

Fig. 10. (a1)–(a4) Texture images, (b1)–(b4) optimal segmentations.

posed algorithm is robust and can segment different textures very well.

5. Conclusion

The analysis of the VTHMRF FCM algorithm described in this paper implies that the proposed algorithm can be viewed as regional and HMRF based, FCM type, fuzzy clustering strategy, to the extent that the algorithm combines the benefits stemming from robust regional and HMRF based segmentation and the increased flexibility of FCM. We presented experimental results to demonstrate the performance of the algorithm, and compared these results with those obtained by the FCM, FCM_S, EnFCM, FGFCM, FLIFCM and HMRF_FCM. Our results for simulated image and real images show that the VHMRF-FCM algorithm performs significantly better than others.

Acknowledgments

This work was supported by the National Natural Science Foundation of China (No. 41301479 and No. 41271435) and the Natural Science Foundation of Liaoning, China (No. 2015020090).

References

[1] T. Acharya, A.K. Ray, Image Processing Principles and Applications, 2005, John Wiley & Sons, Hoboken, 2005.
[2] M.N Ahmed, S.M. Yamany, N. Mohamed, A.A. Farag, T. Moriarty, A modified fuzzy c-means algorithm for bias field estimation and segmentation of MRI data, IEEE Trans. Med. Imag. 21 (3) (2002) 193–199.
[3] J. Besag, On the statistical analysis of dirty pictures, J. Roy. Statist. Soc. B. 48 (3) (2008) 259–302.
[4] J. Bezdek, Pattern Recognition with Fuzzy Objective Function Algorithms, Plenum, New York, 1981.
[5] N. Bouguila, W. ElGuebaly, Discrete data clustering using finite mixture models, Pattern Recognit. 42 (1) (2009) 33–42.
[6] W. Cai, S. Chen, D. Zhang, Fast and robust fuzzy c-means clustering algorithms incorporating local information for image segmentation, Pattern Recognit. 40 (3) (2007) 825–838.
[7] M.C. Chandhok, S. Chaturvedi, A.A. Khurshid, An approach to image segmentation using K-means clustering algorithm, Int. J. Inf. Tech. 1 (1) (2012) 11–17.
[8] S.P. Chatzis, T.A. Varvarigou, A fuzzy clustering approach toward hidden Markov random field models for enhanced spatially constrained image segmentation, IEEE Trans. Fuzzy Syst 16 (5) (2008) 1351–1361.
[9] S. Chen, D. Zhang, Robust image segmentation using FCM with spatial constraints based on new kernel-induced distance measure, IEEE Trans. Syst. Man, Cybern. 34 (4) (2004) 1907–1916.
[10] T. Chen, T.S. Huang, Region based hidden Markov random field model for brain MR image segmentation, World Acad. Sci. Eng. Technol. 1 (4) (2007) 727–730.
[11] G. Chen, T. Hu, X. Guo, X. Meng, A fast region-based image segmentation based on least square method, IEEE Int. Conf. Syst. Man. Cybern (2009) 972–977.
[12] R.G. Congalton, K. Green, Assessing the Accuracy of Remotely Sensed Data: Principles and Practices, CRC Press, FL, Boca Raton, 2008.
[13] E. Cuevas, D. Zaldivar, M. Pérez-Cisneros, A novel multi-threshold segmentation approach based on differential evolution optimization, Expert Syst. Appl. 37 (7) (2010) 5265–5271.
[14] C. Dharmagunawardhana, S. Mahmoodi, M. Bennett, M. Niranjan, Gaussian Markov random field based improved texture descriptor for image segmentation, Image vision Comput. 32 (11) (2014) 884–895.
[15] C. Dharmagunawardhana, S. Mahmoodi, M. Bennett, M. Niranjan, An inhomogeneous Bayesian texture model for spatially varying parameter estimation, in: Proceedings of the International Conference on Pattern Recognition Applications and Methods, 2014, pp. 139–146.
[16] I.L. Dryden, R. Farnoosh, C.C. Taylor, Image segmentation using Voronoi polygons and MCMC, with application to muscle fibre images, J. Appl. Stat. 33 (6) (2006) 609–622.
[17] J.C. Dunn, A fuzzy relative of the ISODATA process and its use in detecting compact well-separated clusters, Cybern. Syst 33 (3) (1973) 32–57.
[18] S. Krinidis, V. Chatzis, A robust fuzzy local information C-means clustering algorithm, IEEE Trans. Image Process 19 (5) (2010) 1328–1337.
[19] H. Ichihashi, K. Miyagishi, K. Honda, Fuzzy C-means clustering with regularization by K-L information, in: 10th IEEE International Conference on Fuzzy Systems, vol. 3, 2001, pp. 924–927.
[20] R. Inokuchi, S. Miyamoto, Fuzzy c-means algorithms using Kullback-Leibler divergence and helliger distance based on multinomial manifold, J. Adv. Comput. Intell. 12 (2) (2008) 443–444.
[21] Y. Li, J. Li, Segmentation of SAR intensity imagery with a reversible jump MCMC algorithm, IEEE Trans. Geosci. Remote Sens. 48 (4) (2010) 1872–1881.
[22] S. Miyamoto, M. Mukaidono, Fuzzy C-means as a regularization and maximum entropy approach, in: Proceedings of the 7th International Fuzzy Systems Association World Congress, 1997, pp. 86–92.
[23] A. Okabe, B. Boots, K. Sugihara, S. Chiu, in: Spatial Tessellations: Concepts and Applications of Voronoi Diagrams, second ed, Chichester: Jonh Wiley & Sons, 2000, p. 676.
[24] L. Szilagyi, Z. Benyo, S.M. Szilagyi, H.S. Adam, MR brain image segmentation using an enhanced fuzzy c-means algorithm, in: Proceedings of the 25th Annual International Conference of the IEEE EMBS, 2003, pp. 17–21.
[25] J. Wang, L. Ju, X. Wang, An edge-weighted centroidal Voronoi tessellation model for image segmentation, IEEE Trans. Image Process 18 (8) (2009) 1844–1858.
[26] L Zadeh, Fuzzy Sets, Inf. Control. 8 (1965) 338–353.
[27] Y. Xia, D.G. Feng, T.J. Wang, R.C. Zhao, Y.N. Zhang, Image segmentation by clustering of spatial patterns, Pattern Recognit. Lett 28 (2007) 1548–1555.